Exploring deazaflavoenzymes as biocatalysts

Kumar, Hemant

3

Isolation and characterization of a thermostable F_{420}:NADPH oxidoreductase from *Thermobifida fusca*

Hemant Kumar*, Quoc-Thai Nguyen*, Claudia Binda, Andrea Mattevi, and Marco W. Fraaije

This chapter is based on *Journal of biological chemistry*, 2017, 292: 10123-10130

*equal authorship

Abstract

$F_{420}H_2$-dependent enzymes reduce a wide range of substrates that are otherwise recalcitrant to enzyme-catalyzed reduction, and their potential for applications in biocatalysis has attracted increasing attention. Thermobifida fusca is a moderately thermophilic bacterium and holds high biocatalytic potential as a source for several highly thermostable enzymes. We report here on the isolation and characterization of a thermostable F_{420}: NADPH oxidoreductase (Tfu-FNO) from T. fusca, the first F_{420}-dependent enzyme described from this bacterium. Tfu-FNO was heterologously expressed in Escherichia coli, yielding up to 200 mg of recombinant enzyme per liter of culture. We found that Tfu-FNO is highly thermostable, reaching its highest activity at 65 °C and that Tfu-FNO is likely to act in vivo as an F_{420} reductase at the expense of NADPH, similar to its counterpart in Streptomyces griseus. We obtained the crystal structure of FNO in complex with $NADP^+$ at 1.8 Å resolution, providing the first bacterial FNO structure. The overall architecture and $NADP^+$-binding site of Tfu-FNO were highly similar to those of the Archaeoglobus fulgidus FNO (Af-FNO). The active site is located in a hydrophobic pocket between an N-terminal dinucleotide binding domain and a smaller C-terminal domain. Residues interacting with the 2 -phosphate of $NADP^+$ were probed by targeted mutagenesis, indicating that Thr-28, Ser-50, Arg-51, and Arg-55 are important for discriminating between $NADP^+$ and NAD^+. Interestingly, a T28A mutant increased the kinetic efficiency >3-fold as compared with the wild-type enzyme when NADH is the substrate. The biochemical and structural data presented here provide crucial insights into the molecular recognition of the two cofactors, F_{420} and NAD(P)H by FNO.

3.1. Introduction

Flavins can arguably be regarded as the most extensively studied redox cofactors. One natural flavin analogue is cofactor F_{420}, which was first isolated and characterized from methanogenic archaea in 1972 (Cheeseman et al. 1972). Since then, F_{420} has been found in members of methanogens, Actinomycetes, Cyanobacteria, and some Betaproteobacteria (Daniels et al. 1985). Replacement of the 5' nitrogen of flavins with a carbon in F_{420}, resulting in a so-called deazaflavin, renders the cofactor nearly unreactive toward molecular oxygen. Hence, F_{420} is an obligate hydride-transfer cofactor similar to the nicotinamide cofactors (Fig. 1). In addition, the 8'-OH group on the isoalloxazine ring in F_{420} has been suggested to slow down the autooxidation of the reduced cofactor ($F_{420}H_2$) in air; thus, the reduced species is much more stable than that of flavins (Jacobson and Walsh 1984).

Many $F_{420}(H_2)$-dependent enzymes have been characterized recently, and their potential for applications in biocatalysis has attracted increasing attention (Taylor et al. 2013; Greening et al. 2016). F_{420}-dependent enzymes studied so far have been shown to be capable of reducing a wide range of substrates that are otherwise recalcitrant to enzyme-catalyzed reduction (Taylor et al. 2013; Greening et al. 2016). However, the commercial unavailability of cofactor F_{420} remains a bottleneck for studying and applying the respective enzymes. Therefore, it would be attrac-tive to have access to an efficient $F_{420}H_2$ cofactor recycling system. In this context, F_{420}:NADPH oxidoreductases (FNOs,3 EC 1.5.1.40; Fig. 1) could become very valuable as NADPH-driven $F_{420}H_2$-recycling systems. FNOs catalyze the reduction of $NADP^+$ using $F_{420}H_2$ and have been found in a number of archaea (Dudley Eirich and Dugger 1984; de Wit and Eker 1987; Kunow et al. 1993; Berk and Thauer 1997; Elias et al. 2000) and bacteria (Eker et al. 1989)(Fig. 1). It has been argued that in methanogens, FNO catalyzes mainly the reduction of $NADP^+$ using $F_{420}H_2$, whereas bacterial FNOs are supposed to catalyze the reverse reaction (Eker et al. 1989).

Thermobifida fusca is a moderately thermophilic soil bacterium with high G + C content. This actinomycete holds high biocatalytic potential as it has already served as a source for several highly thermostable enzymes, e.g. catalase, Baeyer-Villiger monooxygenase, and glycoside hydrolases (Lončar and Fraaije; Wilson 2004; Fraaije et al. 2005). Interestingly, a recent bioinformatic study predicted that the *T. fusca* genome contains 16 genes encoding for F_{420}-dependent enzymes (Selengut and Haft 2010). Nevertheless, there has been so far no biochemical evidence for such enzymes. Here, we describe the identification and characterization of a dimeric thermostable F_{420}:NADPH oxidoreductase from *T. fusca*

(Tfu-FNO), confirming the presence of F_{420}-dependent enzymes in this mesophilic bacterium. Despite the high GC content (67%) of the gene sequence, Tfu-FNO is readily expressed in *Escherichia coli*. Notably, Tfu-FNO is a thermostable enzyme and shows a clear substrate preference toward NADP(H) instead of NAD(H). By solving the three-dimensional crystal structure of Tfu-FNO, we set out site-directed mutagenesis to corroborate the role of residues that interact with the phosphate moiety at 2' position of $NADP^+$.

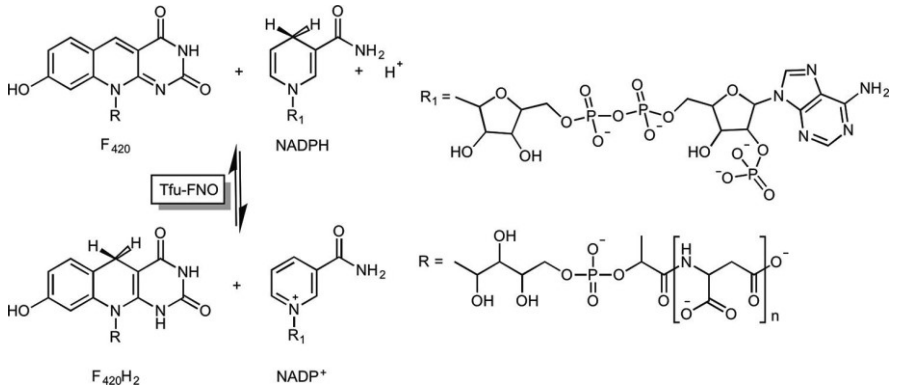

Figure 1. The reversible reaction catalyzed by F_{420}:NADPH oxidoreductase. The number of glutamate residues attached to the phospholactyl moiety may vary (*n* = 2-8 in case of *M. smegmatis*).

3.2. Experimental section

3.2.1. Cloning, expression, and purification of Tfu-FNO

T. fusca YX was grown at 55 °C in Hägerdahl medium, and its genomic DNA was extracted using the GeneElute Bacterial Genomic DNA kit (Sigma). The gene Tfu-*fno* (Tfu_0970, TFU_RS04835) was PCR-amplified from genomic DNA of *T. fusca* using the pair of primers listed in Table 2 with the NdeI and HindIII restriction sites introduced at the 5' and 3' positions of the gene, respectively. The purified PCR product and the pBAD*N*/*Myc*-HisA vector were digested with the restric-tion enzymes NdeI and HindIII, purified, and ligated (vector to insert ratio ca. 1 to 5 (mol/mol)) using T4 DNA ligase (Promega) with quick ligation buffer. The pBAD*N*/*Myc*-HisA vector is a variant of the commercial pBAD/*Myc*-HisA (Invitrogen) where the unique NcoI site at the translation start is replaced with NdeI. The liga-

tion product was transformed into chemically competent *E. coli* TOP10 cells using the heat shock method. Correct transformants were confirmed by sequencing the recombinant plasmid pBAD-*fno*. Site-directed mutagenesis was carried out by using the pBAD-*fno* vector as template and the QuikChange® mutagenesis method with the corresponding pairs of primers listed in Table 2. The primers (200 nM) were used in a 10 *m*l reaction mixture. In the case of the double mutants, plasmids with a single mutation were used as the template. The remaining parent template vector was digested by incubating with DpnI (New England BioLabs) at 37 °C for 2 h. DpnI was then inactivated at 80 °C for 10 min, and the mutant plasmid was transformed into chemically competent *E. coli* TOP10 cells. Mutations were confirmed by sequencing.

***fno* genes**	**Forward primers (5 –3)**	**Reverse primers (5 –3)**
FNO WT	TGC***CATATG***TCGATTGCCGTGCTG TCG	***AAGCTT***TAGATGTCGGTGATGCGGATAC
FNO_R51M	TGATTCTCGGTTCG**ATG**AGCGCGGAGCGGG	CCCGCTCCGCGCT**CAT**CGAACCGAGAATCA
FNO_S50Q	GCACGAGGTGATTCTCGGT**CAG**CGGAGCGCG	CGCGCTCCG**CTG**ACCGAGAATCACCTCGTGC
FNO_S50E	GCACGAGGTGATTCTCGGT**GAG**CGGAGCGCG	CGCGCTCCG**CTC**ACCGAGAATCACCTCGTGC
FNO_R55S	GGAGCGCGGAG**AGC**GCCCAGGCGGT	ACCGCCTGGGC**GCT**CTCCGCGCTCC
FNO_R55N	GCGGAGCGCGGAG**AAC**GCCCAGGCGGTTG	CAACCGCCTGGGC**GTT**CTCCGCGCTCCGC
FNO_T28A	GTGCTGGGGGGC**GCG**GGTGATCAGG	CCTGATCACC**CGC**GCCCCCCAGCAC
FNO_R51A	GATTCTCGGTTCG**GCG**AGCGCGGAGCGG	CCGCTCCGCGCT**CGC**CGAACCGAGAATC
FNO_R51V	GATTCTCGGTTCG**GTG**AGCGCGGAGCGG	CCGCTCCGCGCT**CAC**CGAACCGAGAATC
FNO_R51E	GATTCTCGGTTCG**GAG**AGCGCGGAGCGG	CCGCTCCGCGCT**CTC**CGAACCGAGAATC
FNO_R55A	GGAGCGCGGAG**GCG**GCCCAGGCGG	CCGCCTGGGC**CGC**CTCCGCGCTCC
FNO_R55V	GGAGCGCGGAG**GTG**GCCCAGGCGG	CCGCCTGGGC**CAC**CTCCGCGCTCC
FNO_R55E	GGAGCGCGGAG**GAG**GCCCAGGCGG	CCGCCTGGGC**CTC**CTCCGCGCTCC
FNO_S50A	ACGAGGTGATTCTCGGT**GCG**CGGAGCG	CGCTCCG**CGC**ACCGAGAATCACCTCGT

Table 2: Primers used in this study. Sites of mutations are marked with oligonucleotides in bold, whereas restriction sites are in bold italic.

E. coli TOP10 cells with pBAD-*fno* were grown overnight at 37 °C, 130 rpm in a 5-ml lysogenic broth (LB) containing 50 µg/ml ampicillin. This preculture was used to inoculate 500 ml of the same medium and grown at 37 °C, 130 rpm. When the A_{600} reached 0.4 – 0.6, the protein expression was induced by the addition of 0.02% (w/v) arabinose followed by incubation at 30 °C, 130 rpm for 12 h. Cells were harvested by centrifugation at 6000 *g* for 15 min (JLA 10.500 rotor, 4 °C) and resuspended in 10 ml of 50 mM Kp_i, pH 7.0, supplemented with 1 µg/ml of DNase I. Cells were sonicated for 7 min (10 s on, 15 s off cycle, 70% amplitude) at 4 °C using a VCX130 Vibra-Cell sonicator (Sonics & Materials, Inc., Newton, CT) and then centrifuged at 15000 × *g* (JA 17 rotor) for 45 min to obtain the cell-free extract. Tfu-FNO was precipitated by adding 50% saturated ammonium sulfate followed by anion exchange chromatography with a HiTrap™ Q HP 5 ml (GE Healthcare)

column pre-equilibrated with the same resuspension buffer. Tfu-FNO was eluted by using a linear gradient of 0 – 1 M NaCl in the same buffer. At around 250 mM NaCl, Tfu-FNO started eluting. Excess salt was removed by using a PD-10 desalting column, and the protein was stored in 50 mM Kp_i buffer (GE Healthcare). Protein con-centration was estimated using Bradford assay (Bradford 1976).

3.2.2. Temperature, pH optima, and thermostability of Tfu-FNO

F_{420} was isolated from *M. smegmatis* mc^2 4517 as previously published protocol (Isabelle et al. 2002). $F_{420}H_2$ was prepared by biocatalytic reduction of F_{420} using a recombinant F_{420}-dependent glucose-6-phosphate dehydrogenase from *Rhodococcus jostii* RHA1 (Nguyen et al. 2017) as previously described (Manjunatha et al. 2006). The apparent melting temperature, T_m, was determined using the *Thermofluor*® technique (Pantoliano et al. 2001) with a Bio-Rad C1000 Touch Thermal Cycler (Bio-Rad). The reaction volume was 25 µl, containing 10 µM of enzyme and 5 µl of 5 × SYPRO Orange (Invitrogen). To determine the temperature for optimal activity of Tfu-FNO, the enzyme activity was measured using 1.25 mM NADH and 20 µM F_{420} in 50 mM Kp_i, pH 6.0, in a 100 µl reaction volume. The cuvette containing the substrates in pre-heated buffer was heated to the tested temperature (25 – 90 °C), and the reaction was started by adding 10 nM enzyme. The pH optimum was determined for both the forward and backward reactions of Tfu-FNO. F_{420} depletion at 400 nm (ε_{400} = 25 mM^{-1} cm^{-1}) (Dudley Eirich and Dugger 1984)(Wolfe 1985) or NADH formation at 340 nm (ε_{340} = 6.22 mM^{-1} cm^{-1}) was followed using a V-660 spectrophotometer from Jasco (IJsselstein, The Netherlands). In this experi-ment the reaction (100 µl) contained 250 µM NADPH and 20 µM F_{420} (F_{420} reduction) or 250 µM $NADP^+$ and 20 µM $F_{420}H_2$ ($NADP^+$ reduction) in 50 mM buffer. Sodium acetate, Kp_i, and Tricine-KOH based buffers were used for pH 4.5–5.5, 6.0 –7.5, and 8.0 –9.5, respectively.

3.2.3. Steady-state kinetic analyses

To determine the kinetic parameters of the enzyme, initial F_{420} reduction rates were measured using a SynergyMX micro-plate reader (BioTek) using 96-well F-bottom plates (Greiner Bio-One GmbH) at 25 °C. The reaction was performed in 50 mM Kp_i, pH 6.0, and was started by adding 25 – 50 nM enzyme in the final volume of 200 µl. The concentration of one of the substrates was kept constant (250 µM for NADPH and 20 µM for F_{420}, respectively) while varying the concentration of the other substrate. All the measurements were performed in duplicate. A decrease of absorption either at 400 nm (F_{420} reduction, ε_{400} = 25.7 mM^{-1} cm^{-1}) or at 340 nm (NADPH oxidation, ε_{340} = 6.22 mM^{-1} cm^{-1}) was followed to determine the observed rates, k_{obs} (s^{-1}). K_m and k_{cat} values for $NADP^+$, NADPH, F_{420}, and $F_{420}H_2$ were calculated by fitting the data into the Michaelis-Menten

kinetic model using nonlinear regression with GraphPad Prism 6.00 (GraphPad Software, La Jolla, CA).

3.2.4. Crystallization, X-ray data collection, and structure determination of Tfu-FNO

Native Tfu-FNO was crystallized using the sitting-drop vapor diffusion technique at 20 °C by mixing equal volumes of 9.0 mg/ml protein in 10 mM Tris/HCl, pH 7.5, 100 mM NaCl and of the reservoir solution containing 5% (w/v) PEG 3000, 30% (v/v) PEG 400, 10% (v/v) glycerol, 0.1 M HEPES, pH 7.5. Before data collection, crystals were cryo -protected in the mother liquor and flash-cooled by plunging them into liquid nitrogen. X-ray diffraction data to 1.8 Å were collected at the ID30B beamline of the European Synchrotron Radiation Facility in Grenoble, France (ESRF). Image indexing, integration, and data scaling were processed with XDS package (Kabsch 2010a; Kabsch 2010b) and pro-grams of the CCP4 suite (Pettersen et al. 2004). The Tfu-FNO structure was initially solved by molecular replacement method with Phaser (McCoy et al. 2007) using the coordinates of FNO from *A. fulgidus* (PDB ID code 1JAY; (Warkentin et al. 2001)), which shares 40% sequence identity with Tfu-FNO as a starting model devoid of all ligands and water molecules. Manual model correction and structure analysis was carried out with Coot (Emsley et al. 2004), whereas alternating cycles of refinement was performed with Refmac5 (Murshudov et al. 1997). The figures were generated by using UCSF Chimera (Pettersen et al. 2004). Atomic coordinates and structure factors were deposited in the Protein Data Bank under the accession code 5N2I. Detailed data processing and refinement statistics are available in Table 3.

PDB ID code	5N2I
Space group	$P2_12_12_1$
Resolution (Å)	1.80
a, *b*, *c* (Å)	82.4, 86.1, 136.8
R_{sym}[a,b] (%)	11.2 (99.1)
Completeness[b] (%)	98.6 (90.2)
Unique reflections	89383
Multiplicity[b]	4.5 (2.8)
I/σ[b]	7.9 (0.9)
$CC_{1/2}$[b]	0.99 (0.25)
Number of atoms	
Protein	6594

$NADP^+$/glycerol/water	4 48/7 6/600
Average B value for all atoms ($Å^2$)	25.0
$R_{cryst}^{b,c}$ (%)	16.5 (34.1)
$R_{free}^{b,c}$ (%)	21.4 (35.7)
Root mean square bond length (Å)	0.019
Root mean square bond angles (°)	2.02
Ramachandran outliers	0

Table 3. Data collection and refinement statistics

3.3. Results

3.3.1. Purification of Tfu-FNO

A BLAST search for Af-FNO homologs in *T. fusca* resulted in the identification of the Tfu_0907 gene (TFU_RS04835). The encoded protein shares 40 and 70% sequence identity to FNOs from *Archaeoglobus fulgidus* and *Streptomyces griseus*, respectively (Fig. 2). The Tfu-*fno* gene, with a high GC content (67%), was amplified from the genomic DNA of *T. fusca* and transformed into *E. coli* TOP10 as a pBAD-*fno* construct. Purification of the respective protein, Tfu-FNO, was achieved through ammonium sulfate precipitation followed by anion exchange chromatography. DNase I treatment during the first steps of protein purification was found to be essential to remove residual DNA. Tfu-FNO was obtained in pure form with a relatively high yield: 120 – 200 mg/liter culture. It is worth noting that the amount of purified Tfu-FNO obtained in our system is significantly higher than that of Af-FNO when heterologously expressed in *E. coli* (2 mg/liter culture; (Le et al. 2015)).

3.3.2. Effects of pH and temperature on activity

FNOs are known to catalyze the reduction of $NADP^+$ at higher pH, whereas at lower pH it catalyzes the reverse reaction. Fig. 3 shows the effect of pH on Tfu-FNO activity. The reduction rate of $NADP^+$ is highest at pH 8.5–9.0, whereas the reverse reaction is optimal between pH 4.0 and 6.0. From the k_{obs} values of both the forward and backward reactions, it can be concluded that FNO catalyzes $NADP^+$ reduction more efficiently (Fig. 3). This is in line with the redox potential of F_{420} (340 mV) being lower when compared with that of $NADP^+$ (320 mV) (Jacobson and Walsh 1984).

Because FNO originates from the mesophilic organism *T. fusca*, the enzyme is expected to be stable at relatively high temperatures. Measuring the activities at temperatures between 25 and 90 °C revealed that the enzyme displays highest activity between 60 and 70 °C (Fig. 4). The activity at 65 °C is almost 4 higher than that at 25 °C. The apparent melting temperature of Tfu-FNO was found to be 75 °C, as measured by the *Thermofluor*® method (Pantoliano et al. 2001). All the generated Tfu-FNO mutants had melting temperatures similar to the wild-type enzyme (data not shown). This indicates that FNO is remarkably thermostable and is most active at elevated temperatures.

3.3.3. Steady-state kinetics

The steady-state kinetic parameters were measured for NADPH and F_{420} as substrates by following absorbance of these two cofactors at either 340 nm or 400 nm, respectively. The concentration of one substrate was varied while keeping the other substrate at a constant, saturated concentration. The kinetic data fitted well to the Michaelis-Menten kinetic model when the observed rates (k_{obs}) were plotted against substrate concentrations. Tfu-FNO had a K_m value of 7.3 µM and 2.0 µM for NADPH and F_{420}, respectively, at pH 6.0 and 25 °C (Table 1). Thus, Tfu-FNO has a significantly lower K_m for NADPH (2.0 µM) compared with the values featured by Af-FNO (40 µM) and FNO from S. griseus (19.5 mM) (Eker et al. 1989; Kunow et al. 1993). The k_{cat} (3.3 s^{-1}) of Tfu-FNO was somewhat lower when compared with that of Af-FNO (5.27 s^{-1}) (Hossain et al. 2015).

3.3.4. The overall structure of Tfu-FNO

Crystallization of Tfu-FNO was successful, which allowed the elucidation of its crystal structure. This revealed that $NADP^+$ had been co-purified with the native enzyme, as it was found to be bound in the active site (Figs. 5 and 6). All crystal soaking attempts to obtain the F_{420} cofactor bound in the enzyme active site failed, which can be explained by the tight molecular packing found in Tfu-FNO crystals that would hamper cofactor binding in the same position as found in Af-FNO (Fig. 5*A*). It is known that, depending on the bacterial species, the number of glutamate moieties of F_{420} can vary from two to nine, with five to six being the predominant species in mycobacteria (Bair et al. 2001). Given the crystal arrangement of Tfu-FNO molecules, an oligoglutamate tail of F_{420} of any length would clash against another subunit interacting through crystal packing (Fig. 5*A*). Nevertheless, the architecture of the active site is highly conserved, and $NADP^+$ adopted a virtually identical position with respect to that observed in Af-FNO (Fig. 5*B*). Therefore, F_{420} was tentatively modeled in Tfu-FNO upon superposition of the archaeal enzyme (Fig. 5*C*). The modeled F_{420} fit very well into the Tfu-FNO active site without any clashes. Simi-

larly to Af-FNO, F_{420} would bind in Tfu-FNO at the C-terminal domain with its deazaisoalloxazine ring buried deep inside the catalytic pocket and the highly polar oligoglutamyl tail directed toward the exterior of the dimer (Fig. 5, *B* and *C*).

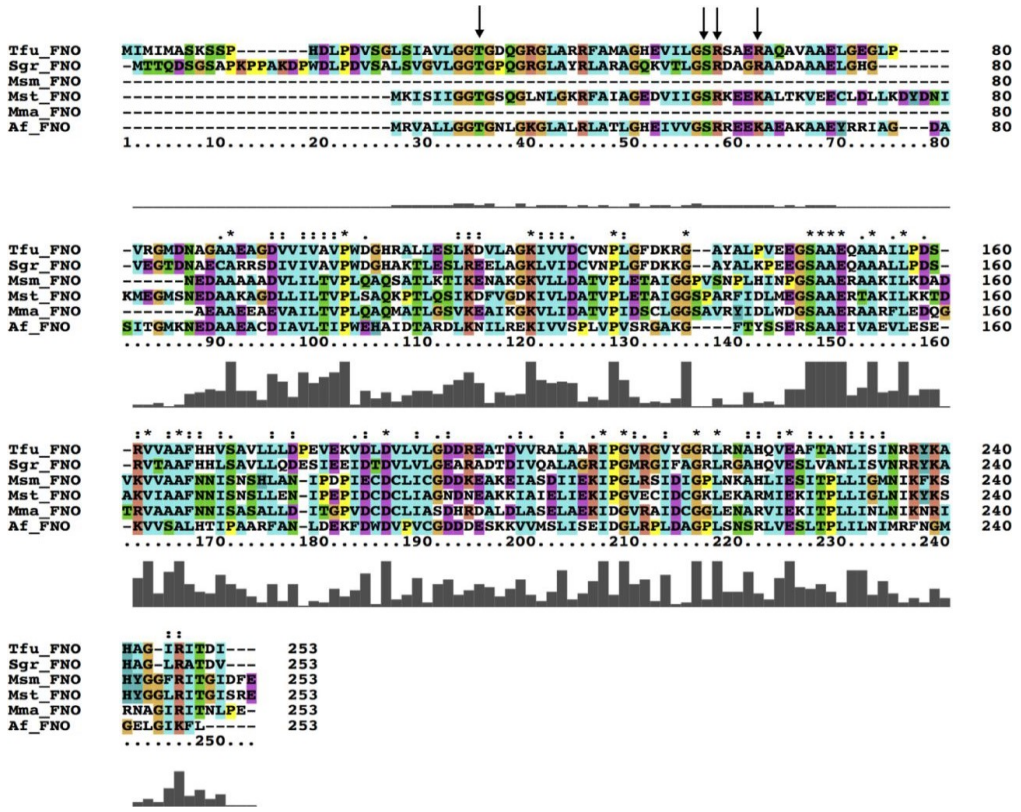

Figure 2. Multiple sequence alignment of selected FNOs from *T. fusca* (*Tfu_FNO*), *A. fulgidus* (*Af_FNO*), *Methanothermobacter marburgensis* (*Mma_FNO*), *Methanobrevibacter smithii* (*Msm_FNO*), *Methanosphaera stadtmanae* (*Mst_FNO*), and *S. griseus* (*Sgr_FNO*). The figure was generated with Clustal X2.1. Residues involved in binding the 2 -phosphate group of $NADP^+$ are indicated with an *arrow*.

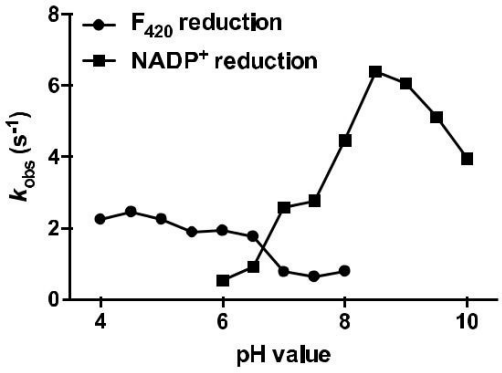

Figure 3. pH optimum for the Tfu-FNO-catalyzed F_{420} reduction using NADPH (*dots*) or the $NADP^+$ reduction using $F_{420}H_2$ (*squares*) at 24 °C. The k_{obs} (s^{-1}) for the $NADP^+$ reduction (pH optima 8 –10) was almost 3 times higher than that for the F_{420} reduction (pH optimum 4 – 6).

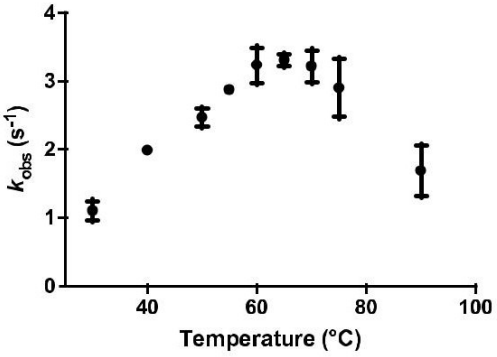

Figure 4. Effect of temperature on Tfu-FNO activity. The reaction mixture of 100 μl contained 1.25 mM NADH, 20 μM F_{420} in 50 mM Kp_i, pH 6.0. The reaction was started by adding 50 nM FNO. The *error bars* represent S.D. from two measurements.

As mentioned above, $NADP^+$ binds to the N-terminal part of Tfu-FNO in a highly similar manner to that of Af-FNO, which is characteristic for members of the dinucleotide-binding protein family (Carugo and Argos 1997; Warkentin et al. 2001). The hydrogen-bonding network between $NADP^+$ and the residues that form the active site are illustrated in Fig. 6. In particular, the nicotinamide ring directly docks to the protein by hydrogen-bonding the cofactor amide group to the peptide nitrogen of Ala-155 (corresponding to Ala-137 in Af-FNO). This conserved interaction is believed to be crucial in conferring the *trans* conformation of the amide group. With this conformation, the pyridine ring of

$NADP^+$ is maintained planar, which in turn facilitates the hydride transfer between the C4 of the $NADP^+$ and C5 of F_{420} by shortening the distance of the two atoms (Warkentin et al. 2001).

3.3.5. $NADP^+$ binding site

The residues involved in binding the ADP moiety are also conserved in Tfu-FNO (Fig. 6). Analogous to Af-FNO, the negatively charged group of the ribose 2' -phosphate interacts with the side chains of Thr-28, Ser-50, Arg-51, and Arg-55 (corresponding to Thr-9, Ser-31, Arg-32, and Lys-36 in Af-FNO). These residues are highly conserved in other known FNOs (Fig. 2). These residues, therefore, appear to be crucial for substrate recognition and help to discriminate between $NADP^+$ and NAD (Warkentin et al. 2001). To get more insights into the role of these residues, they were mutated into amino acids.

Tfu-FNO variant	NADH			NADPH			$k_{cat}/K_{m,NADPH}$/ $k_{cat}/K_{m,\ NADH}$
	K_m (mM)	k_{cat} (s^{-1})	k_{cat}/K_m ($M^{-1}s^{-1}$)	K_m (μM)	k_{cat} (s^{-1})	k_{cat}/K_m ($mM^{-1}s^{-1}$)	
Wild type	14 ± 4.2	2.2 ± 0.4	160	7.3 ± 1.0	3.3 ± 0.1	450	2800
T28A	5.0 ± 0.6	2.6 ± 0.1	520	19 ± 2.6	14 ± 0.5	720	1400
S50E	3.2 ± 1.0	2.7 ± 0.3	840	>500	ND		
S50Q	8.2 ± 2.7	4.2 ± 0.6	510	>500	ND		
R51A	8.6 ± 0.9	3.2 ± 0.2	370	>180	>1.6	6.2	17
R51V	8.7 ± 1.1	3.4 ± 0.2	290	>180	>1.3	9.3	32
R55A	7.0 ± 0.8	3.0 ± 0.2	420	29 ± 4.0	8.8 ± 0.3	300	710
R55N	6.3 ± 3.6	2.8 ± 0.7	440	>500	ND		
R55S	4.4 ± 1.3	3.5 ± 0.4	790	170 ± 38	6.9 ± 0.7	41	52
R55V	9.6 ± 1.4	3.2 ± 0.2	330	49 ± 7.2	ND		
T28A/R55A	5.4 ± 1.5	2.5 ± 0.3	460	93 ± 29	3.3 ± 0.4	3.5	8
T28A/R51V	12 ± 2.2	2.7 ± 0.3	230	>500	ND		
S50E/R55A	20 ± 9.2	2.3 ± 0.7	120	>500	ND		
S50E/R55V	9.8 ± 2.3	1.8 ± 0.2	180	>500	ND		
R51E/R55A	10 ± 2.7	1.6 ± 0.2	160	>500	ND		
R51E/R55N	6.5 ± 1.3	2.7 ± 0.2	420	>500	ND		
R51E/R55S	32 ± 1.9	4.9 ± 0.2	150	>500	ND		
R51V/R55V	10 ± 1.4	2.8 ± 0.2	280	>500	ND		
T28A/R51V/R55V	12 ± 2.2	3.3 ± 0.3	280	>500	ND		

Table 1. Steady-state kinetic parameters for wild-type and mutant Tfu-FNOs using NADH and NADPH as substrate

ND, not determined.

with different charge and/or size and tested for the cofactor specificity toward the two nicotinamide cofactors. Table 1 shows the kinetic parameters for both NADH and NADPH as substrate. For wild-type Tfu-FNO, the K_m value for NADH (14 mM) is several orders of magnitude higher than that for NADPH (7.3 μM), clearly confirming that the enzyme pre-

fers NADP(H) over NAD(H). For all mutants, the K_m value for NADPH significantly increased (from 2.6- to 68-fold) compared with that of the wild-type enzyme, which verified the crucial role of these residues in binding NADP(H) . Intriguingly, recognition of NADH remained the same or improved in all mutants (see Table 3), with a K_m value ranging from 0.23 to 2.3 that from the wild type. Noticeably, R55N and R55S variants have a significantly improved affinity toward NADH. In the case of mutant R55N, $K_{m,\ NADPH}$ increased 100-fold, whereas $K_{m,\ NADH}$ decreased almost 4-fold. The S50E mutant was the best among the tested mutants with a $K_{m,\ NADH}$ of almost 5 lower and a $K_{m,\ NADPH}$ of 100-fold higher as compared with wild-type Tfu-FNO. Interestingly, the T28A mutant showed an increased activity toward both NADPH and NADH, with a 4-fold increase in catalytic rate (k_{cat} 14 s^{-1}) for NADPH and a 2.8-fold decrease in K_m value (5 mM) for NADH when compared with the wild-type enzyme. This resulted in significantly improved k_{cat}/K_m values for both NADPH and NADH, respectively. Unfortunately, combinations of the mutations did not show significant additive effects (Table 1).

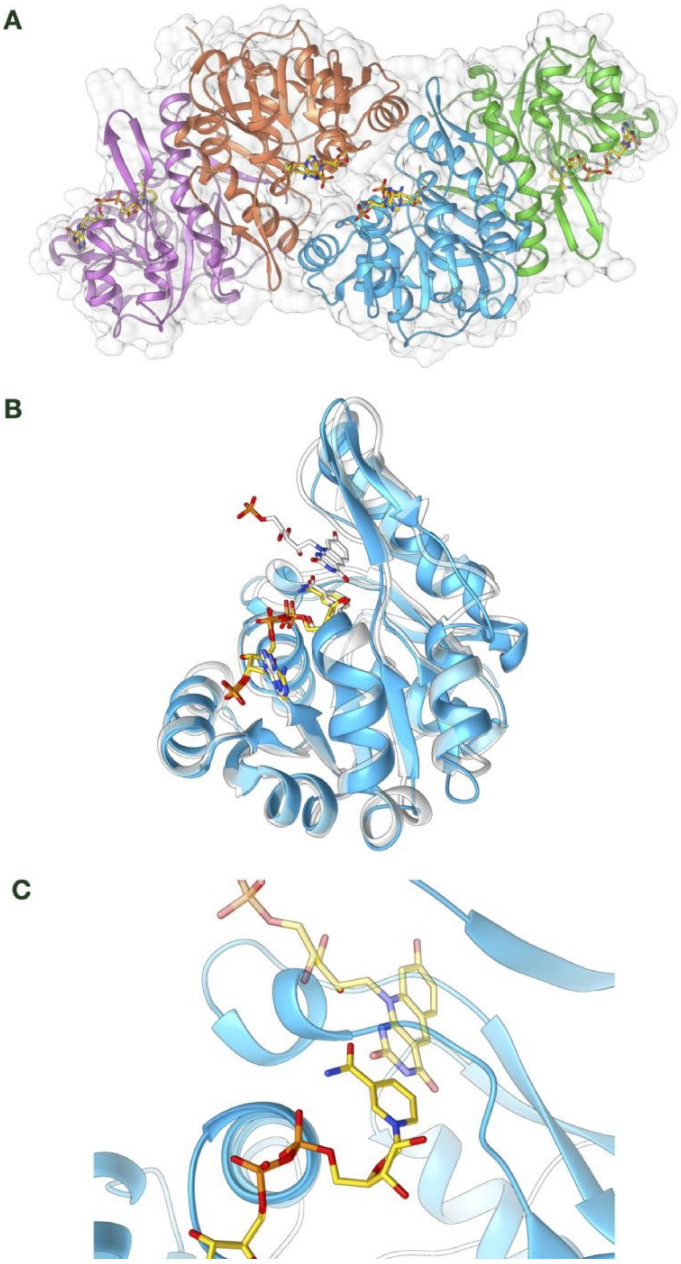

Figure 5. Crystal structure of FNO from *T. fusca*. *A*, the asymmetric unit of Tfu-FNO crystals contains two dimers, AB and CD, colored in *coral* (*monomer A*), *orchid* (*monomer B*), *deep sky blue* (*monomer C*), and *green* (*monomer D*), respectively. *B*, superposition of the Tfu-FNO

monomer C onto the homo-logous $NADP^+$ - and F_{420}-bound Af-FNO monomer (carbon atoms are in *white*, 40% sequence identity, PDB ID 1JAY; Ref. 20). The two structures largely share the same overall topology and the binding pocket architecture, with the nic-otinamide rings adopting a similar position in the active site. *C*, close-up view of Tfu-FNO binding pocket with a modeled F_{420} molecule (in shaded colors with carbon atoms in *yellow*) as a result of superposition as in *B*. The NADP(H) carbon atoms are shown in *yellow*, oxygen atoms in *red*, nitrogen atoms in *blue*, and phosphorous atoms in *orange*.

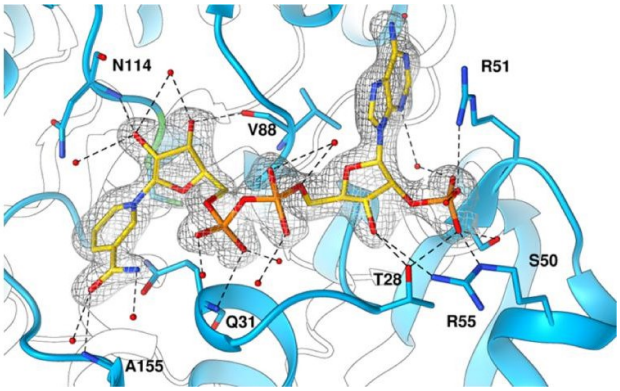

Figure 6. Active site of Tfu-FNO in complex with $NADP^+$. Unbiased $2F_o$ F_c electron density map calculated at 1.8 Å and contoured at 1.0 *s* is drawn as *gray chicken-wire*. Potential hydrogen bonds are depicted with *dashed lines* and water molecules as *red spheres*. Residues in direct contact with $NADP^+$ are labeled. The orientation of the molecule is 180° clockwise rotated along an axis perpendicular to the plane of the paper with respect to that in Fig. 5. Color coding for atoms is as in Figure 5.

3.4. Discussion

F_{420}-dependent enzymes are interesting candidates for biotechnological applications (Taylor et al. 2013). Recent studies have suggested widespread occurrence of such deazaflavin-dependent enzymes in Actinobacteria (Selengut and Haft 2010). Some specific lineages seem especially rich in F_{420}-dependent enzymes, such as *Mycobacterium tuberculosis*. This makes members of this superfamily of deazaflavoproteins potential drug targets due to their absence in the human proteome and the human gut flora. The work of Selengut and Haft (Selengut and Haft 2010) also predicted the presence of at least 16 F_{420}-related genes in *T. fusca*, including all genes required for F_{420} biosynthesis. Through

our study, we experimentally confirmed the presence of an F_{420}-dependent enzyme in this actinomycete by cloning and characterization of a thermostable F_{420}:NADPH oxidoreductase (Tfu-FNO), which catalyzes the reduction of $NADP^+$ using reduced F_{420} and the reverse reaction.

3.4.1. The role of FNO in generating reduced F_{420}

F_{420} cofactor provides microorganism alternative redox pathways. The deazaflavin cofactor seems especially equipped for reduction reactions, as it displays a redox potential that is lower when compared with the nicotinamide cofactor. Two enzymes have been identified in previous studies that serve a role in reducing F_{420}:FNO and F_{420}-dependent glucose-6-phosphate dehydrogenase (FGD) (Greening et al. 2016). Using *T. fusca* cell-free extract and heterologously expressed Tfu_1669 (a putative *M. tuberculosis* FGD homolog), we could not detect any FGD activity. This suggests that the *T. fusca* proteome indeed does not include an FGD. In fact, it has been shown before that not all actinomycetes have an FGD (Purwantini et al. 2006). Therefore, FNO may be the primary enzyme in actinomycetes for providing the cells with $F_{420}H_2$. Nevertheless, at physiological pH (7.0 – 8.0; Fig. 3) Tfu-FNO performs reduction of $NADP^+$ slightly better than reduction of cofactor F_{420}, which is different from the FNO from *S.griseus* (Eker et al. 1989) and more similar to the archaeal FNOs (de Wit and Eker 1987; Kunow et al. 1993) This can partly be explained by the experimental condition (24 °C) differing from the optimum temperature at which the bacteria grow (55 °C) and the intercellular environment (e.g. cofactor concentrations, salt concentrations). Several lines of evidence suggest that in other actinomycetes, such as *Rhodococcus opacus* and *Nocardioides simplex*, FNO is also the main source of $F_{420}H_2$. In these bacteria, the *fno* gene was embedded in the same operon with genes encoding for the $F_{420}H_2$-dependent reductases, which are involved in the metabolism of picrate and 2,4-dinitrophenols (Ebert et al. 1999; Ebert et al. 2001; Knackmuss et al. 2002). FNO-catalyzed regeneration of $F_{420}H_2$ was also proposed to be crucial for the reductive steps in the biosynthesis of tetracycline by *Streptomyces* (NovotnÃ¡ et al. 1989).

3.4.2. Structure and NADP(H) binding site of Tfu-FNO

FNO is believed to be the only F_{420}-dependent enzyme known so far that is conserved between archaea and bacteria (Greening et al. 2016). Except for a 19-amino acid extension loop at the N terminus, Tfu-FNO largely shares the overall topology and cofactor binding site with that from *A. fulgidus* (Figs. 2 and 5*B*). The residues that interact directly with the 2 -phosphate group of NADP(H) are also highly conserved (Fig. 6) and have prov-

en to be essential for binding this cofactor. Upon disrupting the hydrogen-bonding network by mutagenesis, all the mutants lost virtually all ability to recognize NADPH (Table 1). Intriguingly, the affinity of these variants toward NADH improved, with the S50E mutant being the best in terms of specificity for NADH (5.3-fold higher k_{cat}/K_m than that of WT). Yet, an effi-cient NADH-dependent FNO has still to be engineered. For this, a newly developed tool could be explored that can guide structure-inspired switching of coenzyme specificity (Cahn et al. 2016).

3.4.3. Potential applications in biocatalysis

Tfu-FNO represents a highly attractive candidate for the biocatalytic reduction of F_{420}. The enzyme is very thermostable, remains active over a wide range of pH (Figs. 3 and 4), and can be easily expressed in *E. coli* (120 –200 mg/liter culture). Tfu-FNO is also a relatively fast enzyme, especially with the T28A mutant displaying a k_{cat} of 14 s^{-1} for NADPH (Table 1). Whereas the majority of current enzymatic $F_{420}H_2$ regeneration protocols employ FGDs (Manjunatha et al. 2006; Nguyen et al. 2017), the cost of the expensive, non-recyclable cosubstrate glucose-6-phosphate remains the main bottleneck for the use of such enzyme in large-scale applications. Therefore, an $F_{420}H_2$-generating system whose cosubstrate could be recycled, such as T28A Tfu-FNO, would be highly promising. Available, robust NAD(P)H regeneration machineries, such as glucose dehydrogenase or other dehydro-genases, have been thoroughly investigated and widely applied in industry (Wichmann and Vasic-Racki 2005). Therefore, by combining Tfu-FNO with an appropriate NAD(P)H recycler, $F_{420}H_2$ reductases can be exploited for biocatalytic purposes.

Author contributions—H. K. and M. W. F. conceived the study and designed the experiments. H. K. performed the cloning, expression, purification, and biochemical characterization of the Tfu-FNO wild type and variants. Q.-T. N. performed the crystallization and solved the structure of Tfu-FNO under the supervision of A. M. and C. B. H. K. and Q.-T. N. drafted the manuscript. All authors contributed to analyzing the data and writing the paper.

Acknowledgments—We thank the European Synchrotron Radiation Facility (ESRF) for providing beam time and assistance. We are grate-ful to Dr. G. Bashiri at the Structural Biology Laboratory, School of Biological Sciences and Maurice Wilkins Centre for Molecular Bio-discovery, University of Auckland, New Zealand for generously pro-viding a culture of *M. smegmatis* mc^2 4517 and the plasmid pYUB-Duet-FbiABC. A. Giusti, S. Rovida, and F. Forneris are acknowledged for experimental support.

References

Bair TB, Isabelle DW, Daniels L (2001) Structures of coenzyme F_{420} in *Mycobacterium* species. Arch Microbiol 176:37–43.

Berk H, Thauer RK (1997) Function of coenzyme F_{420}-dependent NADP reductase in methanogenic archaea containing an NADP-dependent alcohol dehydrogenase. Arch Microbiol 168:396–402.

Bradford MM (1976) A Rapid and Sensitive Method for the Quantitation of Microgram Quantities of Protein Utilizing the Principle of Protein-Dye Binding. Anal Biochem 72:248–254.

Cahn JKB, Werlang CA, Baumschlager A, Brinkmann-Chen S, Mayo SL, Arnold FH (2016) A General Tool for Engineering the NAD/NADP Cofactor Preference of Oxidoreductases.

Carugo O, Argos P (1997) NADP-dependent enzymes. II: Evolution of the mono- and dinucleotide binding domains. Proteins Struct Funct Genet 28:29–40.

Cheeseman P, Toms-wood A, Wolfe RS (1972) Isolation and Properties of a Fluorescent, Factor$_{420}$, from *Methanobacterium* Strain M.o.H.. Microbiology 112:527–531.

Daniels L, Bakhiet N, Harmon K (1985) Widespread Distribution of a 5-deazaflavin Cofactor in Actinomyces and Related Bacteria. Syst Appl Microbiol 6:12–17.

De Wit LEA, Eker APM (1987) 8-Hydroxy-5-deazaflavin-dependent electron transfer in the extreme halophile *Halobacterium cutirubrum*. FEMS Microbiol Lett 48:121–125.

Dudley Eirich L, Dugger RS (1984) Purification and properties of an F_{420}-dependent NADP reductase from *Methanobacterium thermoautotrophicum*. BBA - Gen Subj 802:454–458.

Ebert S, Fischer P, Knackmuss H-J (2001) Converging catabolism of 2,4,6-trinitrophenol (picric acid) and 2,4-dinitrophenol by Nocardioides simplex FJ2-1A. Biodegradation 12:367–376.

Ebert S, Rieger PG, Knackmuss HJ (1999) Function of coenzyme F_{420} in aerobic catabolism of 2,4, 6-trinitrophenol and 2,4-dinitrophenol by Nocardioides simplex FJ2-1A. J Bacteriol 181:2669–74.

Eker a. PM, Hessels JKC, Meerwaldt R (1989) Characterization of an 8-hydroxy-5-deazaflavin: NADPH oxidoreductase from Streptomyces griseus. Biochim Biophys Acta - Gen Subj 990:80–86.

Elias DA, Juck DF, Berry KA, Sparling R (2000) Purification of the $NADP^+$: F_{420} oxidoreductase of *Methanosphaera stadtmanae*. 420:998–1003.

Emsley P, Cowtan K, IUCr (2004) Model-building tools for molecular graphics. Acta Crystallogr Sect D Biol Crystallogr 60:2126–2132.

Fraaije MW, Wu J, Heuts DPHM, van Hellemond EW, Spelberg JHL, Janssen DB (2005) Discovery of a thermostable Baeyer-Villiger monooxygenase by genome mining. Appl Microbiol Biotechnol 66:393–400.

Greening C, Ahmed FH, Mohamed AE, Lee BM, Pandey G, Warden AC, Scott C, Oakeshott JG, Taylor MC, Jackson J (2016) Physiology, Biochemistry, and Applications of F_{420}- and F_o-Dependent Redox Reactions. Microbiol Mol Biol Rev 80:451–493.

Hossain MS, Le CQ, Joseph E, Nguyen TQ, Johnson-Winters K, Foss FW (2015) Convenient synthesis of deazaflavin cofactor FO and its activity in F_{420}-dependent NADP reductase. Org Biomol Chem 13:5082–5085.

Isabelle D, Simpson DR, Daniels L (2002) Large-scale production of coenzyme F_{420}-5,6 by using *Mycobacterium smegmatis*. Appl Environ Microbiol 68:5750–5.

Jacobson F, Walsh C (1984) Properties of 7,8-didemethyl-8-hydroxy-5-deazaflavins relevant to redox coenzyme function in methanogen metabolism. Biochemistry 23:979–988.

Kabsch W (2010a) Integration, scaling, space-group assignment and post-refinement. Acta Crystallogr Sect D Biol Crystallogr 66:133–144.

Kabsch W (2010b) XDS. Acta Crystallogr Sect D Biol Crystallogr 66:125–132.

Knackmuss H-J, Heiss G, Hofmann KW, Trachtmann N, Rouvière P, Walters DM (2002) *npd* gene functions of *Rhodococcus* (*opacus*) *erythropolis* HL PM-1 in the initial steps of 2,4,6-trinitrophenol degradation. Microbiology 148:799–806.

Kunow J, Schwörer B, Stetter KO, Thauer RK (1993) A F_{420}-dependent NADP reductase in the extremely thermophilic sulfate-reducing *Archaeoglobus fulgidus*. Arch Microbiol 160:199–205.

Le CQ, Joseph E, Nguyen T, Johnson-Winters K (2015) Optimization of expression and purification of recombinant *Archeoglobus fulgidus* $F_{420}H_2$:$NADP^+$ Oxidoreductase, an F_{420} cofactor dependent enzyme. Protein J 34:391–397.

Lončar N, Fraaije MW Not so monofunctional-a case of thermostable *Thermobifida fusca* catalase with peroxidase activity.

Manjunatha UH, Boshoff H, Dowd CS, Zhang L, Albert TJ, Norton JE, Daniels L, Dick T, Pang SS, Barry CE (2006) Identification of a nitroimidazo-oxazine-specific protein involved in PA-824 resistance in *Mycobacterium tuberculosis*. Proc Natl Acad Sci U S A 103:431–436.

McCoy AJ, Grosse-Kunstleve RW, Adams PD, Winn MD, Storoni LC, Read RJ (2007) *Phaser* crystallographic software. J Appl Crystallogr 40:658–674.

Murshudov GN, Vagin AA, Dodson EJ (1997) Refinement of macromolecular structures by the maximum-likelihood method. Acta Crystallogr Sect D Biol Crystallogr 53:240–255.

Nguyen QT, Trinco G, Binda C, Mattevi A, Fraaije MW (2017) Discovery and characterization of an F_{420}-dependent glucose-6-phosphate dehydrogenase (Rh-FGD1) from *Rhodococcus jostii* RHA1. Appl Microbiol Biotechnol 101:2831–2842.

Novotná J, Neužil J, Hošťálek Z (1989) Spectrophotometric identification of 8-hydroxy-5-deazaflavin: NADPH oxidoreductase activity in S*treptomycetes* producing tetracyclines. FEMS Microbiol Lett 59:241–245.

Pantoliano MW, Petrella EC, Kwasnoski JD, Lobanov VS, James Myslik EG, Carver T, Asel E, Springer BA, Lane P, Salemme FR (2001) High-density miniaturized thermal shift assays as a general strategy for drug discovery. J Biomol Screen 6:429–440.

Pettersen EF, Goddard TD, Huang CC, Couch GS, Greenblatt DM, Meng EC, Ferrin TE (2004) UCSF Chimera - A visualization system for exploratory research and analysis. J Comput Chem 25:1605–1612.

Purwantini E, Gillis TP, Daniels L (2006) Presence of F_{420}-dependent glucose-6-phosphate dehydrogenase in *Mycobacterium* and *Nocardia* species, but absence from *Streptomyces* and *Corynebacterium* species and methanogenic Archaea. FEMS Microbiol Lett 146:129–134.

Selengut JD, Haft DH (2010) Unexpected abundance of coenzyme F_{420}-dependent enzymes in

Mycobacterium tuberculosis and other actinobacteria. J Bacteriol 192:5788–98.

Taylor M, Scott C, Grogan G (2013) F_{420}-dependent enzymes-potential for applications in biotechnology. Trends Biotechnol 31:63–4.

Warkentin E, Mamat B, Sordel-Klippert M, Wicke M, Thauer RK, Iwata M, Iwata S, Ermler U, Shima S (2001) Structures of $F_{420}H_2$:$NADP^{(+)}$ oxidoreductase with and without its substrates bound. Embo J 20:6561–6569

Wichmann R, Vasic-Racki D (2005) Cofactor Regeneration at the Lab Scale. Springer, Berlin, Heidelberg, pp 225–260

Wilson DB (2004) Studies of *Thermobifida fusca* plant cell wall degrading enzymes. Chem Rec 4:72–82.

Wolfe RS (1985) Unusual coenzymes of methanogenesis. Trends Biochem Sci 10:396–399.